Research Article | Vol. 32, No. 17 / 12 Aug 2024 / Optics Express 30326

Optics EXPRESS

Femtosecond laser plane-by-plane inscription of ultra-short DBR fiber lasers for sensing applications

RUNXIAO CHEN,[1,2] XIZHEN XU,[1,2,3] JIAFENG WU,[1,2] JIA HE,[1,2] YING WANG,[1,2,3] CHANGRUI LIAO,[1,2,3] YIPING WANG,[1,2,3] AND JUN HE[1,2,3,*]

[1] *State Key Laboratory of Radio Frequency Heterogeneous Integration, Key Laboratory of Optoelectronic Devices and Systems of Ministry of Education/Guangdong Province, College of Physics and Optoelectronic Engineering, Shenzhen University, Shenzhen 518060, China*
[2] *Shenzhen Key Laboratory of Ultrafast Laser Micro/Nano Manufacturing, Guangdong and Hong Kong Joint Research Centre for Optical Fibre Sensors, Shenzhen University, Shenzhen 518060, China*
[3] *Guangdong Laboratory of Artificial Intelligence and Digital Economy (SZ), Shenzhen 518107, China*
[*] *hejun07@szu.edu.cn*

Abstract: We propose and demonstrate the inscription of ultra-short distributed Bragg reflector fiber lasers (DBR-FLs) in Er/Yb co-doped fiber (EYDF) using a femtosecond laser plane-by-plane (Pl-b-Pl) method. By integrating the spherical aberration (SA) with a laser 2D scanning process, a planar refractive index modification (RIM) region can be induced in the fiber core. Thanks to the Pl-b-Pl inscription, a high-quality fiber Bragg grating (FBG) in an EYDF is produced, exhibiting a grating strength exceeding 40 dB and an insertion loss of 0.1 dB. Subsequently, an ultra-short DBR-FL with an entire length of 7.3 mm is fabricated by the Pl-b-Pl inscription. The Pl-b-Pl ultra-short DBR-FL exhibits an improved slope efficiency of 0.7% compared with the DBR-FLs fabricated using another two direct-writing techniques, namely line-by-line (LbL) and point-by-point (PbP) methods. Furthermore, this ultra-short DBR-FL generates single-frequency and single-polarization radiation with a narrow linewidth (9.4 kHz) and a low relative intensity noise (-105.8 dB/Hz). Moreover, a wavelength-division-multiplexed array consisting of eight ultra-short DBR-FLs with distinct lasing wavelengths is successfully created. The Pl-b-Pl ultra-short DBR-FLs with excellent output performances offer significant potential for high-sensitivity sensing applications requiring high spatial resolution.

1. Introduction

Fiber Bragg grating (FBG) lasers with single-frequency and single-polarization radiation have been developed as attractive sensing elements due to their distinct advantages including narrow linewidth, high signal-to-noise ratio (SNR), and multiplexing capability [1–3]. Thanks to these superior characteristics, FBG laser sensors integrated with interferometric interrogation techniques enable significantly enhanced sensitivity in sensing applications compared to the passive FBG sensors [3,4]. Generally, the typical length for both distributed feedback fiber lasers (DFB-FLs) and distributed Bragg reflector fiber lasers (DBR-FLs) spans several centimeters [5–7]. However, for specific applications such as nuclear reactor cores, gastrointestinal imaging, and lithium-ion batteries etc., where compact point sensors are required, the use of long linear-cavity lasers may be impractical [8–10]. In addition, the fabrication and packaging processes of the long structure become more challenging resulting from its susceptibility to localized perturbations and uneven force distributions. To address these problems, efforts have been made on the fabrication of short linear-cavity lasers. For instance, Guan *et al.* employed a 193 nm excimer laser and a phase mask to fabricate DBR-FLs in Er/Yb co-doped fibers (EYDFs) with an entire laser length

#532441 https://doi.org/10.1364/OE.532441
Journal © 2024 Received 11 Jun 2024; revised 21 Jul 2024; accepted 29 Jul 2024; published 6 Aug 2024

Optics EXPRESS

of only 8.4 mm [11]. Using the same method, Wong *et al.* reported the fabrication of ultra-short DBR-FLs with 7 mm in length in Er-doped fibers (EDFs) [12]. However, due to the intrinsic and UV-induced birefringence of the fiber, the UV-written DBR-FLs without any post-processing are prone to operate with two orthogonal polarization modes, which leads to phase instability of the interferometric demodulated signals [13]. Notably, single-frequency and single-polarization DBR-FLs can be directly fabricated by using a femtosecond (fs) laser and a phase mask [14–16]. Nevertheless, the multiplexing capacity of DBR-FLs fabricated by the phase mask method is inherently limited by the fixed period of the phase mask. Various techniques, including defocusing lenses, spatial light modulators (SLMs), deformable mirrors, and strain-induced stretching, have been employed for the wavelength tuning of FBGs using a single phase mask [17–20]. However, these methods are constrained by the limited tuning range of the Bragg wavelength. Consequently, it is difficult to create a DBR-FL wavelength-division-multiplexed array using the phase mask method.

Femtosecond laser direct-writing techniques, including point-by-point (PbP), line-by-line (LbL) and plane-by-plane (Pl-b-Pl) methods, have been demonstrated to be more flexible for fabricating FBGs with different Bragg wavelengths and complex spectral designs such as phase shift, chirp and apodization etc. [21–24]. To date, FBG lasers produced by fs laser direct-writing techniques have attracted great interest. For example, in 2006, Lai *et al.* firstly proposed the fs laser PbP inscription of single-frequency DBR-FLs in EYDFs [25]. The DBR-FLs were operated in the single-polarization region, resulting from the significant birefringence induced by the fs laser pulses. In addition, Babin *et al.* further developed the PbP method to fabricate extremely short (5.3 mm) DFB-FLs in heavily doped EDFs, offering a single-frequency and single-polarization radiation with a narrow linewidth of 3.5 kHz [26]. Furthermore, fs laser LbL direct-writing method was reported for fabricating single-frequency and single-polarization DFB-FLs, generating a narrow laser linewidth of sub-kHz [27]. However, the typical PbP and LbL FBGs exhibit relatively high scattering loss (i.e., 2 dB and 0.5 dB for PbP and LbL FBGs in Ref. [27]), which leads to a decreased slope efficiency (SE) for the FBG lasers. Notably, the employment of fs laser Pl-b-Pl inscriptions has the potential to optimize the insertion loss (IL) [22]. For example, Lu *et al.* proposed the fs laser Pl-b-Pl inscription of FBG using a cylindrical lens, obtaining a grating strength of 25 dB and an IL below 0.02 dB [28]. Recently, we have reported the inscription of high-quality FBGs by a fs laser Pl-b-Pl technology based on the spherical aberration (SA) technique [29]. The planar refractive index modification (RIMs) with homogeneous cross-section can effectively reduce the broadband loss and meanwhile enhance the coupling strength, which thereby holds the potential for inscribing short FBGs with a high reflectivity.

In this paper, we demonstrate the inscription of ultra-short DBR-FLs in EYDFs, for the first time to our knowledge, using a fs laser Pl-b-Pl method. Firstly, the spectral quality of the FBG inscribed in an EYDF is investigated, demonstrating an ultra-high grating coupling strength coefficient κ of $12.6\,\mathrm{cm}^{-1}$. Subsequently, by inscribing a high reflector (HR) and an output coupler (OC) in the EYDF, an ultra-short DBR-FL with an entire length of 7.3 mm is successfully fabricated. For comparison, we have also fabricated DBR-FLs using the fs laser PbP and LbL methods. It turns out that the Pl-b-Pl DBR-FL presents an improved SE. Furthermore, a generation of single-frequency and single-polarization radiation with a narrow linewidth (9.4 kHz) and a low relative intensity noise (-105.8 dB/Hz) is demonstrated for the ultra-short DBR-FL. Moreover, the multiplexing capacity of the DBR-FL is investigated, achieving a wavelength-division-multiplexed array consisting of eight DBR-FLs. The Pl-b-Pl ultra-short DBR-FLs with excellent output performance are attractive for high-sensitivity sensing applications.

2. Experimental setup for DBR-FLs inscription

The gain medium selected for the fabrication of ultra-short DBR-FLs is a commercial EYDF (EY305, Coractive), which has a peak absorption of 1250 dB/m at the 975 nm, offering high gain to the fiber laser. This choice can avoid the ion clustering phenomenon commonly encountered in high-concentration EDFs, which cause self-pulsation and thus instability in the laser [30]. The DBR-FL was fabricated by directly inscribed two wavelength-matched FBGs (a HR and an OC) in a segment of coating-removed EYDF by a fs laser Pl-b-Pl method. The schematic for the inscription of DBR-FLs is displayed in Fig. 1. A frequency-doubled fs laser (Pharos PH1-10, Light Conversion) with a central wavelength of 513 nm, pulse width of 290 fs, repetition rate of 200 kHz is employed. The laser beam is focused through a 3-mm silica plate and into the fiber core using a dry objective (50×, NA = 0.5, Leica). The EYDF is mounted on a glass slide and covered by the silica plate. In addition, index-matching oil is filled between the silica plate and the glass slide to eliminate the distortion arising from the surface curvature of the EYDF. All of them are mounted on high-precision translation stages (X: ABL10100-LN; Y: ABL10100-LN; Z: ANT130 V 5-CN1-PL2, Aerotech), and hence, grating pattern could be written by accurately moving the stages. Notably, the silica plate plays an important role in the Pl-b-Pl inscription process, as it is utilized to introduce spherical aberration (SA) effect for the inscription of DBR-FLs. The SA occurs when the tightly focused laser propagates through the interfaces of air-silica plate and silica plate-EYDF, resulting from the mismatched refractive-index between two different materials [31]. The focal region could be further elongated along the laser propagation direction with a distance between focused position of marginal beam and paraxial beam due to the SA effect [32,33]. Generally, the RIM inscribed by the PbP technique without SA is localized in the fiber core, as shown in the inset (a) of Fig. 1. Subsequently, with the introduction of SA effect to the PbP inscription, LbL inscription is realized as the length of RIM along z axis can be extended up to tens of micrometers by a single laser pulse, as shown in the inset (b) of Fig. 1. Furthermore, by integrating the SA effect with a 2D scanning process along the y-axis and x-axis, enlarged planar RIMs that cover the fiber core can be generated, as illustrated in the inset (c) of Fig. 1.

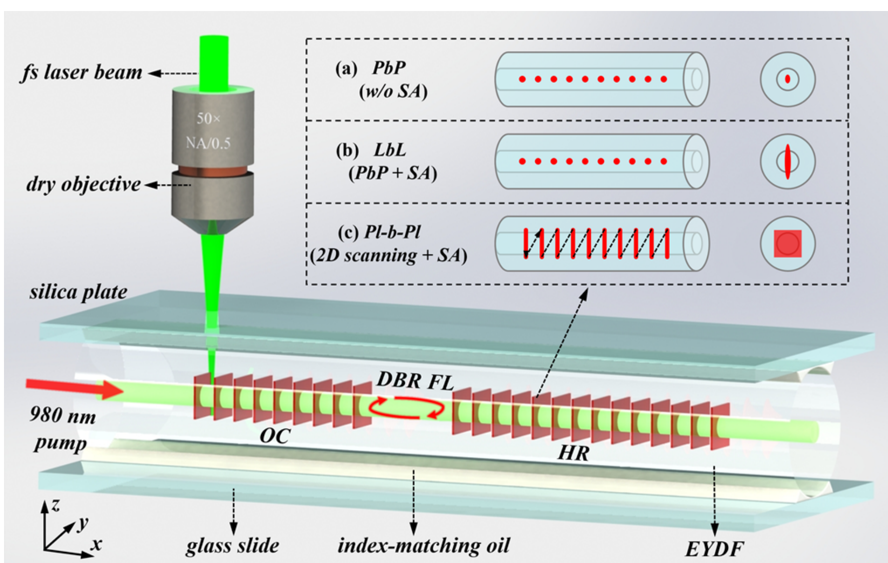

Fig. 1. Experimental setup for DBR-FLs inscription by fs laser Pl-b-Pl method. (Insets: schematic diagrams of the (a) PbP, (b) LbL, and (c) Pl-b-Pl direct-writing inscriptions.

3. Experimental results and discussions

Before the inscription of DBR-FLs, we firstly investigated the spectrum quality of the FBG inscribed in the EYDF. The grating period, scanning length, pulse energy and the writing speed were set as 1.059 µm, 16 µm, 60 nJ and 0.2 mm/s, respectively. During the inscription process, the transmission spectrum was monitored using a broadband source (BBS, Fiberlake) and an optical spectrum analyzer (OSA, Yokogawa). Notably, the transmission spectrum of the FBG was measured by subtracting a reference spectrum of the BBS and thus made the baseline as zero. Therefore, the grating strength and IL could be accurately estimated from the transmission spectrum. As shown in Fig. 2 (a), as the grating length increases, the grating strength enhances while the 3-dB bandwidth decreases. Note that a grating strength more than 40 dB at the Bragg wavelength 1537.22 nm and an IL of 0.1 dB was achieved by a 3.8-mm FBG. Such significant grating strength and low broadband loss observed are attributed to the induced Type-I RIMs, which are characterized by homogeneous modulated planes that cover the fiber core. In addition, the ratio of the coupling strength coefficient to the scattering loss coefficient κ/α is crucial to determine the spectrum quality of an FBG [34]. Notably, κ and α could be calculated as $\kappa = In(T_B)/(-2\ L)$ and $\alpha = In(T_{IL})/(-2\ L)$, where T_B and T_{IL} and L are the Bragg resonance attenuation, insertion loss and grating length of an FBG. As shown in Fig. 2 (b), it is clearly observed that κ and κ/α of the FBG increase with increasing grating length. Note that the maximum κ and κ/α is 12.3 cm^{-1} and 430 at a grating length of 3.8 mm, which indicates an excellent spectrum quality for such a short FBG.

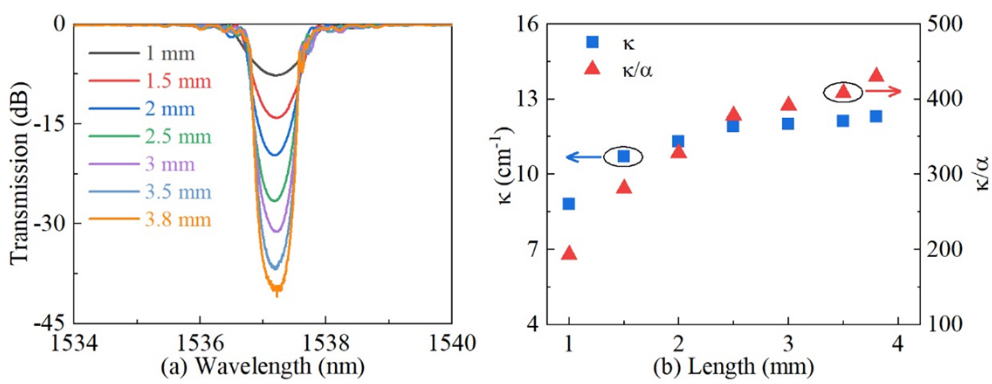

Fig. 2. (a) Measured transmission spectra of the FBG at different lengths; (b) values of κ and κ/α for the FBG at different lengths.

In the experiment, the total length of EYDF used for the preparation of DBR-FL is ~13 mm. The HR in the DBR-FL is 3.3 mm in length, which presents a grating strength of ~35 dB. Subsequently, we began to inscribe an OC with a spacing of 1.8 mm from the HR. During the inscription process, we turned off the BBS and injected the 980 nm pump light into the EYDF through a 980/1550 nm wavelength division multiplexer (WDM). And meanwhile, the backward output spectrum of the DBR-FL was real-time monitored. We then stopped the fabrication process as the output power reached a maximum value, at which point a 2.2-mm long OC with an estimated grating strength ~24 dB was obtained. Consequently, an ultra-short DBR-FL (i.e., S1) with an entire length of 7.3 mm was fabricated. The top- and lateral-view microscope images of the DBR-FL were acquired by a visual acquisition system consisting of a CMOS (STC-MBA1002POE, Omron) and an objective (100×, NA = 1.25, Leica), as shown in Fig. 3(a1) and 3(b1), respectively. It is observed that planar RIMs with a width of 16 µm and a depth of 10 µm were generated. In addition to the transmission spectrum, the reflected BBS spectrum from the DBR-FL was also measured utilizing a circulator, as shown in Fig. 3(c1). A narrow peak appears in the center of the transmission band, corresponding to the lasing wavelength of the DBR-FL. However, the spectra exhibit obscure grating strength in transmission, which is limited by the resolution (0.02 nm) of the OSA. In addition, the IL of such a DBR-FL is estimated to be 0.12 dB.

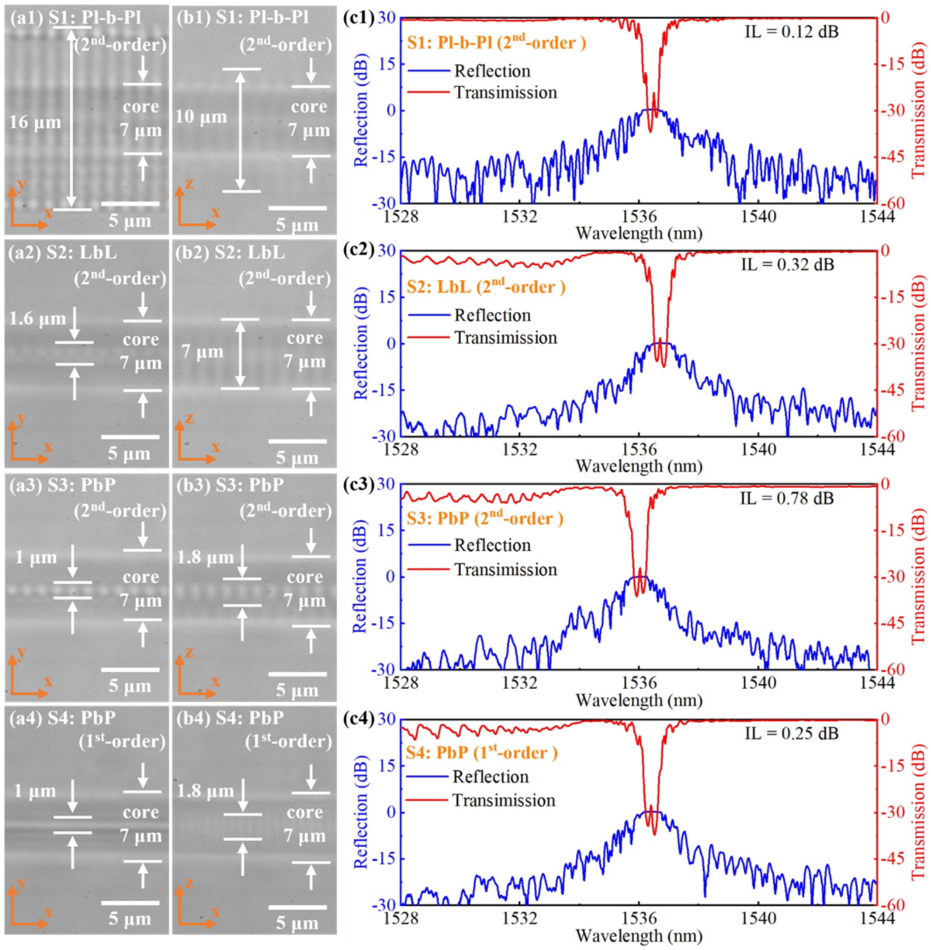

Fig. 3. Four DBR FLs S1-S4 with different RIMs (i.e., plane, line and points for 2^{nd}-order and 1^{st}-order FBG) inscribed by three femtosecond direct-writing techniques. (a) Top-view microscope images; (b) lateral-view microscope images; (c) measured transmission and reflection spectra.

For comparison, we have also fabricated ultra-short DBR-FLs S2-S4 by the fs laser LbL and PbP method. Here, we fabricated the LbL DBR-FL (i.e., S2) using a PbP method based on the SA technique without a scanning process. In addition, we employed an oil- immersion objective (100×, NA = 1.25, Leica) for the fabrication of the PbP DBR-FLs S3 and S4, which were constructed by 2^{nd}-order and 1^{st}-order FBGs, respectively. The total length of EYDF, grating position, grating length and spacing for the LbL and PbP DBR-FLs are identical to S1. Different pulse energies of 400 nJ, 50 nJ and 30 nJ were used for inscribing S2-S4, respectively, resulting in a similar coupling strength with S1. Consequently, the effective length of the cavity for three types of DBR-FLs is similar. As exhibited in Figs. 3(a2)–3(a4) and Figs. 3(b2)–3(b4), the diameter of the modulated spot for S2 is larger (1.6 μm) than that of S3 and S4 (1 μm).

Optics EXPRESS

Furthermore, the lateral-views show that the RIMs of S2 cross the fiber core in the z-direction with a depth of 7 μm, whereas S3 and S4 exhibit shorter depths of 1.8 μm. These differences between the LbL and PbP DBR-FLs are due to the introduction of SA effect and the objectives with different NAs. Moreover, note that S2-S4 present similar grating strength and one peak in the center of the transmission band, as shown in Figs. 3(c2)–3(c4). However, the ILs for S2-S4 are different, which are measured to be 0.32, 0.78 and 0.25 dB for S2-S4, respectively. Among DBR-FLs S1-S4 fabricated by the three direct-writing methods, S1 presents the lowest IL, attributed to the Pl-b-Pl inscription.

Furthermore, a 980-nm pump light was injected into the DBR-FLs S1-S4 through a 980/1550 nm wavelength division multiplexer (WDM). The laser backward output power versus the input pump power was measured, as plotted in Fig. 4(a). It is observed that the output power increases with increasing input power, and the lasing threshold power for S1-S4 is 2, 5, 16 and 3.5 mW, respectively. Furthermore, linear fittings were performed on the original datasets, offering SEs of 0.7%, 0.3%, 0.30% and 0.45% for S1-S4. Note that the SE value of S1, inscribed by the Pl-b-Pl methods, is highest among S1-S3. Conversely, the PbP DBR-FL S3 presents the lowest SE, while the LbL DBR-FL S2 exhibits an intermediate SE value. However, the PbP DBR-FL S4, constructed by 1st-order FBGs, exhibits a higher SE than S2 and S3. These results indicate that the SE of the DBR-FL is primarily impacted by the IL. Therefore, the highest SE for DBR-FL S1 is due to its lowest IL among S1-S4, in accordance with Foster's theory [35]. Moreover, the backward output spectra of the DBR-FLs at a pump power of 60 mW was recorded, as shown in Fig. 4(b). The inset shows the photograph of the lasing ultra-short DBR-FL S1, in which the two darker sections are the HR and OC, respectively. It is observed the lasing wavelength of S1-S4 is 1536.40, 1536.68, 1536.08, and 1536.28 nm with corresponding SNR of 67, 63, 43 and 65 dB, respectively. The measured output power for S1-S4 is 396, 163, 2 and 248 μW, respectively. As a result, the ultra-short DBR-FLs inscribed by the Pl-b-Pl method generates a lower IL compared to that inscribed by the other two direct-writing methods, and thus enabling an improved SE and maximum output power for the laser.

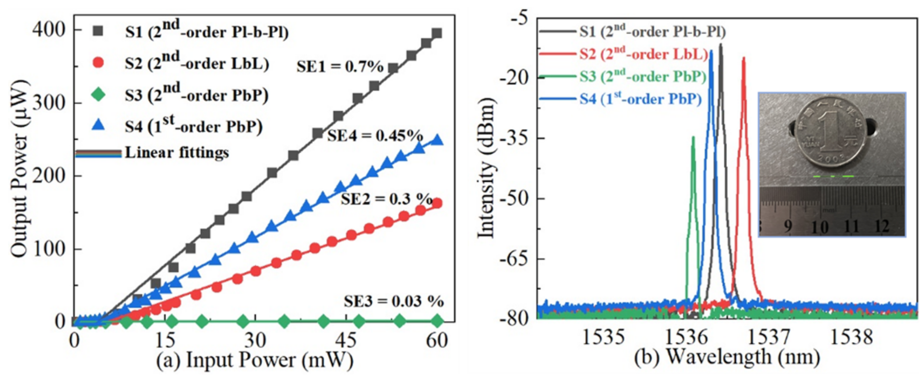

Fig. 4. DBR-FLs S1-S4 fabricated by different direct-writing methods. (a) Laser backward output power versus the input pump power; (b) laser backward output spectra, the inset shows the photograph of the ultra-short DBR-FL S1.

Moreover, the longitudinal mode characteristics, state of polarization, laser linewidth and relative intensity noise (RIN) of the Pl-b-Pl ultra-short DBR-FL were investigated. Firstly, a scanning Fabry-Perot interferometer (SA200-12B, Thorlabs) with a free spectral range (FSR) of 1.5 GHz and a resolution of 7.5 MHz was employed to measure the longitudinal mode characteristics. As shown in Fig. 5(a), a set of stable peaks were detected in a scanning period, indicating that the laser operates in the single-longitudinal-mode region. Subsequently, two methods were adopted to study the polarization characteristics of the DBR-FL. Note that the DBR-FL must be kept straight without any external perturbation on the laser during the measurement process. Firstly, the radio-frequency spectrum of the laser within the range of 0 to 12 GHz was measured by a photodetector (PDA05CF2, Thorlabs) and an electrical spectrum analyzer (N9030B, Keysight), as shown in Fig. 5(b), in which no polarization beat signal is observed. Moreover, a stable point appears on the Poincare sphere and a degree of polarization (DOP) of 0.997 was measured using a polarization analyzer (N7786B, Keysight), as shown in the inset of Fig. 5(b), which indicates that there is no polarization modes competition and the laser operates in a nearly complete linear polarization state. As a result, it was demonstrated that the laser operates in a single-polarization region. In addition, the laser linewidth was measured using a delayed self-heterodyne method [7]. A Lorentz fitting was performed on the measured data, as shown in Fig. 5(c). To avoid the 1/f noise, the laser linewidth is determined by taking 1/20 of the 20-dB bandwidth (188 kHz) at the beat peak, which estimates to be 9.4 kHz. Furthermore, the RIN of the laser was measured by the photodetector and electrical spectrum analyzer, as shown in Fig. 5(d). Note that the RIN is –105.8 dB/Hz at the relaxation oscillation frequency 0.98 MHz.

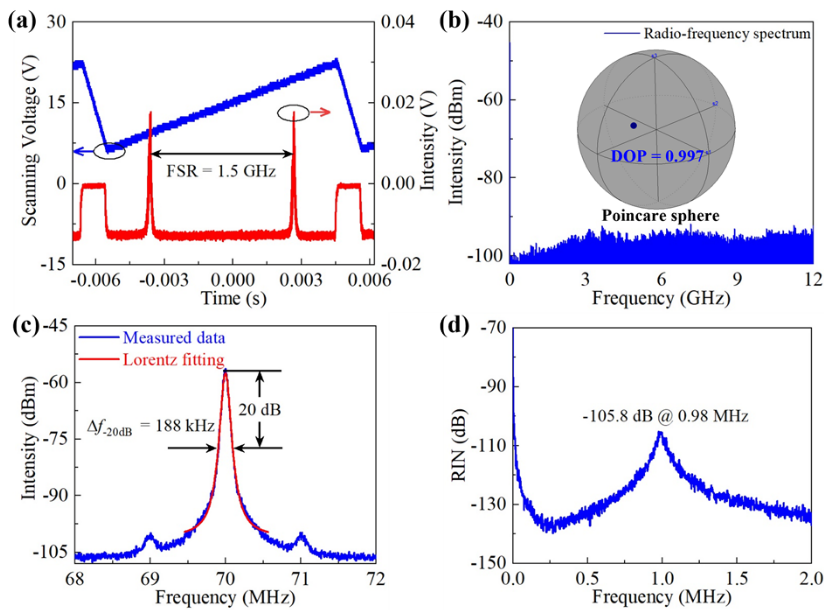

Fig. 5. (a) Longitudinal mode characteristics; (b) state of polarization (SOP); (c) laser linewidth; and (d) relative intensity noise (RIN) of the Pl-b-Pl ultra-short DBR-FL.

We have also investigated the multiplexing capability of the ultra-short DBR-FL fabricated by the fs laser Pl-b-Pl method. A DBR-FL array has been fabricated, which is constructed by eight DBR-FLs with distinct grating periods ranging from 1.056 to 1.068 μm. The lasers were serially spliced in ascending order of the grating period. The output spectrum of the DBR-FL array was measured at a pump power of 500 mW, as exhibited in Fig. 6. Note that eight lasing wavelengths ranging from 1534-1548 nm are simultaneously observed. In addition, the first DBR-FL in the array presents a maximum SNR of 66 dB, while the last one exhibits a minimum SNR of 47 dB. The decreasing trend of SNR is attributed to the successive absorption of the pump power. Fluctuations in the intensity can be observed in the spectrum, which may due to slight variations in the grating coupling strength and IL. As a result, an ultra-short DBR-FL wavelength-division-multiplexed array with eight FL elements is successfully created by the fs laser Pl-b-Pl method, which provides a new approach for multiplexing a large scale of DBR-FL sensors.

Optics EXPRESS

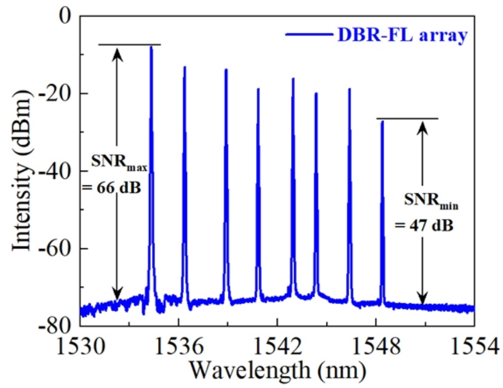

Fig. 6. Lasing spectrum of the DBR-FL array consisting of eight DBR-FLs.

4. Conclusion

We have proposed and demonstrated the fabrication of ultra-short DBR-FLs by a fs laser Pl-b-Pl method. An ultra-short DBR-FL with an entire length of 7.3 mm was successfully inscribed in the EYDF. Notably, an improved SE was achieved for the Pl-b-Pl DBR-FL compared with the DBR-FLs fabricated by the PbP and LbL methods. In addition, it is demonstrated the ultra-short DBR-FL operates in a single-frequency and single-polarization region with a narrow linewidth (9.4 kHz) and a peak RIN of -105.8 dB/Hz at 0.98 MHz. Moreover, a wavelength-division-multiplexed array consisting of eight ultra-short DBR-FLs was successfully created. As a result, the ultra-short DBR-FLs inscribed by the fs laser Pl-b-Pl method present excellent output performance and multiplexing capability, which are promising for high-sensitivity sensing applications requiring high spatial resolution.

Funding. National Natural Science Foundation of China (62222510, 62375176); National Key Research and Development Program of China (2023YFB3208600); Guangdong Provincial Department of Science and Technology (2022B1515120050); Shenzhen Key Laboratory of Ultra-fast Laser Micro/Nano Manufacturing (ZDSYS20220606100405013).

Disclosures. The authors declare no conflicts of interest.

Data availability. Data underlying the results presented in this paper are not publicly available at this time but may be obtained from the authors upon reasonable request.

References

1. C. Spiegelberg, J. H. Geng, Y. D. Hu, *et al.*, "Low-noise narrow-linewidth fiber laser at 1550 nm (June 2003)," J. Lightwave Technol. **22**(1), 57–62 (2004).
2. D. J. Hill, B. Hodder, J. De Freitas, *et al.*, "DFB fibre-laser sensor developments," in *17th International Conference on Optical Fibre Sensors, Proceedings of SPIE* 2005, 904–907.
3. G. A. Cranch, G. M. H. Flockhart, and C. K. Kirkendall, "Distributed feedback fiber laser strain sensors," IEEE Sens. J. **8**(7), 1161–1172 (2008).
4. A. D. Kersey, T. A. Berkoff, and W. W. Morey, "FIBEROPTIC BRAGG GRATING STRAIN SENSOR WITH DRIFT-COMPENSATED HIGH-RESOLUTION INTERFEROMETRIC WAVELENGTH-SHIFT DETECTION," Opt. Lett. **18**(1), 72–74 (1993).
5. J. T. Kringlebotn, J. L. Archambault, L. Reekie, *et al.*, "ER3 + YB3+ CODOPED FIBER DISTRIBUTED-FEEDBACK LASER," Opt. Lett. **19**(24), 2101–2103 (1994).
6. L. Dong, W. H. Loh, J. E. Caplen, *et al.*, "Efficient single-frequency fiber lasers with novel photosensitive Er/Yb optical fibers," Opt. Lett. **22**(10), 694–696 (1997).
7. K. Guo, J. He, K. Yang, *et al.*, "Symmetric Step-Apodized Distributed Feedback Fiber Laser With Improved Efficiency," IEEE Photonics J. **11**(4), 1 (2019).
8. M. A. S. Zaghloul, M. Wang, S. Huang, *et al.*, "Radiation resistant fiber Bragg grating in random air-line fibers for sensing applications in nuclear reactor cores," Opt. Express **26**(9), 11775–11786 (2018).
9. Y. Liang, W. Fu, Q. Li, *et al.*, "Optical-resolution functional gastrointestinal photoacoustic endoscopy based on optical heterodyne detection of ultrasound," Nat. Commun. **13**(1), 1 (2022).

10. W. Mei, Z. Liu, C. Wang, *et al.*, "Operando monitoring of thermal runaway in commercial lithium-ion cells via advanced lab-on-fiber technologies," Nat. Commun. **14**(1), 1 (2023).
11. Y. Zhang, B.-O. Guan, and H.-Y. Tam, "Ultra-short distributed Bragg reflector fiber laser for sensing applications," Opt. Express **17**(12), 10050–10055 (2009).
12. A. C. L. Wong, D. Chen, H.-J. Wang, *et al.*, "Extremely short distributed Bragg reflector fibre lasers with sub-kilohertz linewidth and ultra-low polarization beat frequency for sensing applications," Meas. Sci. Technol. **22**(4), 1 (2011).
13. A. D. Kersey, M. J. Marrone, and A. Dandridge, "Analysis of input-polarization-induced phase noise in interferometric fiber-optic sensors and its reduction using polarization scrambling," J. Lightwave Technol. **8**(6), 838–845 (1990).
14. X. Pham, J. Si, T. Chen, *et al.*, "Ultra-short DBR fiber laser with high-temperature resistance using tilted fiber Bragg grating output coupler," Opt. Express **27**(26), 38532–38540 (2019).
15. R. D. Lv, T. Chen, X. T. Pham, *et al.*, "High-temperature linearly polarized single-frequency fiber lasers based on a non-polarization-maintaining FBG preparation through a femtosecond laser," Opt. Lett. **47**(16), 4111–4114 (2022).
16. R. D. Lv, T. Chen, J. Huang, *et al.*, "Fabrication of Integrated Single Frequency DBR Fiber Laser Directly on YDF by Femtosecond Laser," IEEE Photonics Technol. Lett. **35**(24), 1319–1322 (2023).
17. C. Voigtländer, R. G. Becker, J. Thomas, *et al.*, "Ultrashort pulse inscription of tailored fiber Bragg gratings with a phase mask and a deformed wavefront Invited," Opt. Mater. Express **1**(4), 633–642 (2011).
18. C. Voigtländer, R. G. Krämer, T. A. Goebel, *et al.*, "Variable wavefront tuning with a SLM for tailored femtosecond fiber Bragg grating inscription," Opt. Lett. **41**(1), 17–20 (2016).
19. T. A. Goebel, C. Voigtländer, R. G. Krämer, *et al.*, "Flexible femtosecond inscription of fiber Bragg gratings by an optimized deformable mirror," Opt. Lett. **42**(20), 4215–4218 (2017).
20. J. Habel, T. Boilard, J. S. Frenière, *et al.*, "Femtosecond FBG Written through the Coating for Sensing Applications," Sensors **17**(11), 1 (2017).
21. A. Martinez, M. Dubov, I. Khrushchev, *et al.*, "Direct writing of fibre Bragg gratings by femtosecond laser," Electron. Lett. **40**(19), 1170–1172 (2004).
22. K. Zhou, M. Dubov, C. Mou, *et al.*, "Line-by-Line Fiber Bragg Grating Made by Femtosecond Laser," IEEE Photonics Technol. Lett. **22**(16), 1190–1192 (2010).
23. A. Theodosiou, A. Lacraz, M. Polis, *et al.*, "Modified fs-Laser Inscribed FBG Array for Rapid Mode Shape Capture of Free-Free Vibrating Beams," IEEE Photonics Technol. Lett. **28**(14), 1509–1512 (2016).
24. J. He, B. Xu, X. Xu, *et al.*, "Review of Femtosecond-Laser-Inscribed Fiber Bragg Gratings: Fabrication Technologies and Sensing Applications," Photonic Sens. **11**(2), 203–226 (2021).
25. Y. Lai, A. Martinez, I. Khrushchev, *et al.*, "Distributed Bragg reflector fiber laser fabricated by femtosecond laser inscription," Opt. Lett. **31**(11), 1672–1674 (2006).
26. M. I. Skvortsov, A. A. Wolf, A. A. Vlasov, *et al.*, "Advanced distributed feedback lasers based on composite fiber heavily doped with erbium ions," Sci. Rep. **10**(1), 14487 (2020).
27. W. Sun, J. Shi, Y. Yu, *et al.*, "All-fiber 1.55 µm erbium-doped distributed-feedback laser with single-polarization, single-frequency output by femtosecond laser line-by-line direct-writing," OSA Continuum **4**(2), 334–344 (2021).
28. P. Lu, S. J. Mihailov, H. Ding, *et al.*, "Plane-by-Plane Inscription of Grating Structures in Optical Fibers," J. Lightwave Technol. **36**(4), 926–931 (2018).
29. J. Wu, X. Xu, C. Liao, *et al.*, "Optimized femtosecond laser direct-written fiber Bragg gratings with high reflectivity and low loss," Opt. Express **31**(3), 3831–3838 (2023).
30. A. M. Smirnov and O. V. Butov, "Pump and thermal impact on heavily erbium-doped fiber laser generation," Opt. Lett. **46**(1), 86–89 (2021).
31. J. He, J. F. Wu, X. Z. Xu, *et al.*, "Femtosecond Laser Plane-by-Plane Inscription of Bragg Gratings in Sapphire Fiber," J. Lightwave Technol. **41**(22), 7014–7020 (2023).
32. S. H. Wiersma, P. Torok, T. D. Visser, *et al.*, "Comparison of different theories for focusing through a plane interface," J. Opt. Soc. Am. A **14**(7), 1482–1490 (1997).
33. Q. Sun, H. B. Jiang, Y. Liu, *et al.*, "Effect of spherical aberration on the propagation of a tightly focused femtosecond laser pulse inside fused silica," J. Opt. A: Pure Appl. Opt. **7**(11), 655–659 (2005).
34. X. Xu, J. He, J. He, *et al.*, "Slit Beam Shaping for Femtosecond Laser Point-by- Point Inscription of High-Quality Fiber Bragg Gratings," J. Lightwave Technol. **39**(15), 5142–5148 (2021).
35. S. Foster, "Spatial mode structure of the distributed feedback fiber laser," IEEE J. Quantum Electron. **40**(7), 884–892 (2004).